

Excitation and emission thermal shifts in $ABF_3:Mn^{2+}$ perovskites: coupling with impurity vibrational modes

This article has been downloaded from IOPscience. Please scroll down to see the full text article.

1995 J. Phys.: Condens. Matter 7 7535

(<http://iopscience.iop.org/0953-8984/7/38/012>)

View [the table of contents for this issue](#), or go to the [journal homepage](#) for more

Download details:

IP Address: 171.66.16.151

The article was downloaded on 12/05/2010 at 22:10

Please note that [terms and conditions apply](#).

Excitation and emission thermal shifts in $\text{ABF}_3:\text{Mn}^{2+}$ perovskites: coupling with impurity vibrational modes

M C Marco de Lucas, F Rodríguez and M Moreno

Departamento de Ciencias de la Tierra y Física Materia Condensada, Facultad de Ciencias, Universidad de Cantabria, 39005 Santander, Spain

Received 13 April 1995, in final form 18 May 1995

Abstract. The thermal shifts undergone by the first moment of the ${}^6\text{A}_{1g}(\text{S}) \rightarrow {}^4\text{T}_{1g}(\text{G})$ excitation band and the associated emission band of Mn^{2+} -doped ABF_3 perovskites are investigated in the 9–300 K temperature range. It is found that these shifts are similar for the whole series and have average values of +150 and +450 cm^{-1} for excitation and emission, respectively. Both the sign and the magnitude of these *different* thermal shifts are explained in terms of (i) the phonon assistance mechanism required to gain intensity of the parity-forbidden transitions, (ii) the quadratic electron–phonon coupling and (iii) thermal expansion effects. To achieve this analysis a previous discussion upon the nature of the vibrational modes seen in the optical spectra is carried out. It is stressed that the impurity vibrational mode displaying $\hbar\omega_g = 570 \text{ cm}^{-1}$ in the emission spectrum of $\text{KMgF}_3:\text{Mn}^{2+}$ exhibits a value of 540 cm^{-1} in the corresponding excitation spectrum. This situation, which is also found for other modes seen in the optical spectra of $\text{KMgF}_3:\text{Mn}^{2+}$, indicates that the mode (though associated with the LO_3 branch of KMgF_3) is not a *pure* mode of the lattice but displays a kind of resonant character. As a salient feature the calculated thermal shifts are based on the experimental shifts experienced by the frequencies of the optical and acoustic modes on going from the ground ${}^6\text{A}_{1g}$ to the excited ${}^4\text{T}_{1g}$ state of MnF_6^{4-} . At variance with findings for the *R* lines in Cr^{3+} and V^{2+} , it is clearly demonstrated that the explicit and implicit contributions to the thermal shift of the zero-phonon line in MnF_6^{4-} are similar and both induce red shifts upon heating. Moreover the present analysis reveals that the explicit contribution to the thermal shift undergone by the zero-phonon line of $\text{KMgF}_3:\text{Mn}^{2+}$ is mainly dominated by the odd-parity low-energy modes. The calculated thermal shifts reproduce reasonably well the experimental data.

1. Introduction

The microscopic origin of the thermal shift undergone by crystal field bands of transition metal complexes is still a subject of intensive investigations, which deserves precise analysis in order to clarify the different mechanisms involved in such shifts. Let us designate by $E(T)$ the temperature dependence of the band maximum. Pioneering theories [1–5] related $E(T) - E(0)$ to the vibrational energy. So it was proposed that

$$E(T) - E(0) \propto \hbar\omega_{\text{eff}}n_{\text{eff}} \quad \text{or} \quad \propto \int_0^{\omega_D} \hbar\omega\rho(\omega)n(\omega) d\omega$$

depending on whether a local description with one effective vibrational mode of energy $\hbar\omega_{\text{eff}}$ or an extended phonon state model was considered. Both descriptions are able to explain roughly the thermal band shifts by proper selection of the parameters of the model, which are often obtained by fitting procedures. However, the main problem for a precise understanding of the thermal shifts is to *explain* the values of these parameters in terms of

microscopic models. Nowadays, theoretical studies as well as experiments in this field are focused on determining the relevance of the different mechanisms involved in the thermal shift, such as the contribution from thermal expansion effects or from high-order terms of the electron-phonon interaction hamiltonian. If a detailed microscopic characterization of the thermal shifts is not a simple task for sharp peaks like the R lines of $\text{Al}_2\text{O}_3:\text{Cr}^{3+}$ [6] or $\text{MgO}:\text{V}^{2+}$ [7], this characterization is even harder for electric dipole (ED) transitions in centrosymmetric complexes, involving changes of the electronic configuration from the ground state, $e_g^n t_{2g}^m$, to other excited ones: $e_g^{n-1} t_{2g}^{m+1}$ or $e_g^{n+1} t_{2g}^{m-1}$. In such cases, the thermal shift is strongly influenced not only by the phonon assistance mechanism required to gain ED oscillator strength but also by the thermal expansion, since the transition energy depends directly on the ligand field strength described by the $10Dq$ parameter. In particular, this latter aspect is difficult to take into account when dealing with doped materials, unless the local structure around the impurity is known. Apart from a proper characterization of the linear electron-phonon coupling responsible for the phonon sideband, the analysis of thermal shift for this kind of transition requires a precise knowledge of the nature of the odd-parity vibrations involved in the transition mechanism as well as of the variation of the zero-phonon line (ZPL) induced either by the changes of the thermal population at constant volume (explicit contribution) or by changes in R due to the thermal expansion of the complex (implicit contribution). In the usual cases, this is a complex problem to overcome given that these transitions involve broad absorption or emission bands for which the observation of vibronic fine structure and ZPLs is, in the best case, only possible at low temperatures.

Thermal shifts have been widely investigated for sharp peaks involving spin-flip transitions such as the ${}^4A_2 \rightarrow {}^2E$ in ruby [4] or $\text{MgO}:\text{Cr}^{3+}$ [3] and V^{2+} [8]. Since these transitions are almost independent of $10Dq$, their intensity is mostly concentrated in the ZPL, and the implicit contribution of the thermal shift is much smaller than those for broad bands. Recent estimates of such contributions for the R lines in $\text{MgO}:\text{Cr}^{3+}$ [6] and V^{2+} [7] indicate that the implicit shift is about $+5 \text{ cm}^{-1}$ in the 4–300 K range, which must be compared with the total shift of -17 cm^{-1} experienced by the peak in the same temperature range. Thus the explicit contribution represents about the 80% of the thermal shift.

The aim of the present work is to investigate the temperature dependence of the ${}^6A_{1g} \rightarrow {}^4T_{1g}$ excitation band and the corresponding luminescence band of Mn^{2+} impurity placed in the series KMgF_3 , KZnF_3 , RbCdF_3 , RbCaF_3 and CsCaF_3 fluoroperovskites. Also spectroscopic data [9] from the pure KMnF_3 and RbMnF_3 perovskites are included for comparison purposes. The temperature range where experiments have been carried out is 9–300 K. The emphasis will be placed on explaining the sign and the values of these variations rather than on the shape of their temperature dependence, which nearly follows hyperbolic cotangent functions like $E(T) = E(0) + A \coth(\hbar\omega_{\text{eff}}/2kT)$ or the corresponding Debye-type function. This characteristic behaviour, which can also account for the thermal dependence of either the vibrational lattice energy, $E_{\text{vib}}(T)$, or the variation of interatomic distances by thermal expansion, $R(T)$, could explain why some scientists interpret band shifts either through the variations of $10Dq$ by changes in R due to thermal expansion effects or mainly by explicit contributions like for the V^{2+} or Cr^{3+} R lines. The thermal shifts of the first ${}^4T_{1g} \rightarrow {}^6A_{1g}$ absorption band observed in MnCl_2 [10] and in RbMnF_3 and KMnF_3 [11, 12] were explained in terms of these two extreme behaviours, respectively. Given that, in both cases, $E(T)$ obeys the same thermal statistics, an adequate interpretation of these shifts necessarily requires a detailed analysis of the different contributions.

The selection of the fluoroperovskite series for this work is due to the following reasons: (1) The MnF_6^{4-} complexes, which are responsible for the electronic spectra, display a

perfect O_h symmetry at room temperature. This symmetry is kept at low temperatures even in crystals undergoing structural phase transitions like $RbCdF_3$ ($T_c = 124$ K) [13] and $RbCaF_3$ ($T_{c1} = 193$ K and $T_{c2} = 40$ K) [14]. In particular, the tetragonal distortion, $\Delta R = R_{ax} - R_{eq} = 0.011$ Å displayed by the CdF_6^{4-} octahedra at 30 K, is only 0.002 Å for MnF_6^{4-} as demonstrated by the analysis of ENDOR data reported by Studzinski and Spaeth [15]. (2) The presence of isolated Mn^{2+} in the doped crystals prevents migration processes responsible for the extrinsic luminescence in concentrated compounds [5]. (3) The local structure around the Mn^{2+} is known for the whole series. In particular, the actual Mn–F distance, R , of the MnF_6^{4-} unit embedded in the whole fluoroperovskite series has been determined through the analysis of EPR and optical parameters [16]. (4) The temperature dependence of the lattice parameter, $a(T)$, is known for different fluoroperovskites [16]. (5) A salient feature concerning the present crystals is the observation of ZPLs in the low-temperature luminescence spectra. This result was important to establish the R dependence of the ZPL energy, which exhibits a linear behaviour in the 2.06–2.16 Å range, with $\partial E_{ZPL}/\partial R = +18700$ cm $^{-1}$ Å $^{-1}$ [16]. (6) The low-temperature excitation [17] and luminescence [18] spectra of the $KMgF_3:Mn^{2+}$ crystal display a rich vibronic structure, which provides suitable information about the vibrational frequencies of the coupled modes for the electronic ground state as well as for the ${}^4T_{1g}$ excited one. This information becomes *fundamental* to perform quantitative estimations of the explicit contribution to the thermal shifts. (7) We have made precise measurements of the whole excitation and luminescence bands associated with the first ${}^4T_{1g}$ state in the 9–300 K temperature range in order to determine thermal shifts from moment analysis. It is also noteworthy that the use of Mn^{2+} cations is advantageous for exploring thermal shifts because the ${}^6A_{1g} \rightarrow {}^4T_{1g}$ excitation band is far away from other excited states, at variance with the ${}^4A_2 \rightarrow {}^4T_2$ band in weak-field Cr^{3+} complexes, where the presence of Fano resonances makes it difficult to perform such an analysis.

As pointed out in section 3.1, the thermal shifts are connected with the changes experienced by the frequencies of impurity vibrational modes on passing from the ground state to an excited state. Thus because of the importance played by these impurity modes, a discussion about their nature is given in section 3.2.

2. Experimental results

Table 1 collects the values of the more relevant optical parameters together with some structural data of the $ABF_3:Mn^{2+}$ crystal series. It is worth noting that in the present case we give the values of the first moments, M_{1em} and M_{1ex} , instead of the band maxima E_{em} and E_{ex} reported in previous works [16]. A fundamental reason for this choice is that moments are more directly calculated than band maxima in the theoretical microscopic models. Moreover, its use also avoids errors in the thermal shift measurement when this is made from the band maxima. In particular, these errors can be important if the band shows rich vibrational structure or the bandshape changes with temperature. However, it must be noticed that, in the present case, moments have been calculated directly upon the measured intensity, $I(\omega)$, without any instrumental correction. Although this procedure may induce some deviations in the absolute values of the moments, it gives suitable results when we analyse *variations of moments* induced either by temperature or by changing the host crystal. For the present crystals, we estimate the absolute error of the first moment to be about 100 cm $^{-1}$ though the values, M_{1em} and M_{1ex} , can be measured with an accuracy of 20 cm $^{-1}$. The experiments were performed for the whole $ABF_3:Mn^{2+}$ series employing the

Table 1. Experimental values (cm^{-1}) of the emission and excitation first moment, M_{1em} and M_{1exc} , and bandwidths, H_{exc} and H_{em} , of the ${}^6A_{1g}(S) \leftrightarrow {}^4\Gamma_{1g}(G)$ transition of Mn^{2+} at $T = 300$ K and low temperature along the $\text{ABF}_3:\text{Mn}^{2+}$ series. The R_L , R and ΔR_L values (\AA) are the host B-F distance, the Mn-F distance and the variation of the B-F distance from low temperature to 300 K, respectively. Zero-phonon energies, E_{ZPL} , are taken from [16]; τ (ms) is the experimental low-temperature lifetime; and $\hbar\omega_{\text{eff}}(\text{cm}^{-1})$ is the energy of the effective vibrational mode derived by fitting the experimental $\tau(T)$ values to the equation $\tau(T) = \tau(0) \tanh(\hbar\omega_{\text{eff}}/2kT)$. Estimated errors for the moments are $\pm 20 \text{ cm}^{-1}$.

Compound	T	R_L	R	ΔR_L	M_{1exc}	E_{ZPL}	M_{1em}	H_{exc}	H_{em}	τ ($T = 9$ K)	$\hbar\omega_{\text{eff}}$
KMgF ₃	300	1.993	2.070	—	18 250		16 850				
	9				18 100	17 222	16 400			186	220
KZnF ₃	300	2.026	2.080	0.006	18 620		17 000				
	9				18 500	17 509	16 600			143	260
KMnF ₃	300	2.095	2.095	0.008	18 900		Non-lumin.				
	4.2				18 760	17 883	Extrinsic				
RbMnF ₃	300	2.120	2.120	0.006	19 300		Non-lumin.				
	4.2				19 120	18 221	Extrinsic				
RbCdF ₃	300	2.200	2.130	0.007	19 590		17 780	1240	1760		
	9				19 380	18 360	17 260	950	1330	135	265
RbCaF ₃	300	2.227	2.132	0.008	19 600		17 790	1315	1800		
	9				19 460	18 428	17 290	1020	1390	169	310
CsCaF ₃	300	2.262	2.155	0.008	20 050		18 240	1370	1830		
	9				19 920	18 935	17 850	1060	1370	156	280

Table 2. Excitation and emission thermal shift, ΔE_{ex} and ΔE_{em} , symmetric and antisymmetric parameters, δ_s and δ_a , at 300 and 9 K and their corresponding variations, $\Delta\delta_s(300)$ and $\Delta\delta_a(300)$ (equations (2) and (3)) obtained from the data of table 1 for the $\text{ABF}_3:\text{Mn}^{2+}$ series. Average values are given in the bottom. $\hbar\omega_{\text{eff}}^{\text{gr}}$ and $\hbar\omega_{\text{eff}}^{\text{ex}}$ are the effective phonon energies for the ground and the excited state, respectively, derived from the temperature dependence of the bandwidth (see text). Units in cm^{-1} .

Compound	T (K)	ΔE_{ex}	ΔE_{em}	δ_s	δ_a	$\Delta\delta_s$	$\Delta\delta_a$	$\hbar\omega_{\text{eff}}^{\text{gr}}$	$\hbar\omega_{\text{eff}}^{\text{ex}}$
KMgF ₃	300	150	450	17 550	700	300	-150		
	9			17 250	850				
KZnF ₃	300	120	400	17 810	810	260	-140		
	9			17 550	950				
RbCdF ₃	300	210	520	18 685	905	365	-155	281	271
	9			18 320	1060				
RbCaF ₃	300	140	500	18 695	905	320	-180	290	287
	9			18 375	1085				
CsCaF ₃	300	130	390	19 145	905	260	-130	288	264
	9			18 885	1035				
Average	300	150	450			300	-150		
σ		30	50			40	20		

same procedure as described elsewhere [13, 14, 16]. The results are summarized in tables 1 and 2.

Inspection of table 1 shows that (1) both the excitation and emission bands shift to higher energies upon heating. The corresponding energy shifts, $\Delta E_i(300) = M_{1i}(300) - M_{1i}(9)$ ($i = em$ or ex), for emission are *higher* than for excitation, $\Delta E_{em}(T) > \Delta E_{ex}(T)$, at any

temperature along the whole series. These shifts are similar for all crystals and have average values $\Delta E_{em}(300) = 450 \text{ cm}^{-1}$ and $\Delta E_{ex}(300) = 150 \text{ cm}^{-1}$, irrespective of R (table 2). In this way, it must be pointed out that R mainly influences the transition energy for each crystal but not its thermal shift. (2) The radiative lifetime at low temperature ranges from 135 to 186 ms. Its temperature dependence follows hyperbolic tangent functions characteristic of ED phonon-assisted transitions with effective phonon energies, $\hbar\omega_u \approx 200\text{--}300 \text{ cm}^{-1}$ [13, 14, 18]. These values are similar to those spectroscopically obtained from the ED peaks at low temperature. (3) The variation of the Mn–F distance, $\Delta R(T) = R(T) - R(9)$, at 300 K is taken as $\Delta R(300) = 0.007 \text{ \AA}$ for all crystals. Although $\Delta R(300)$ has not been measured at the impurity level, this value is very similar to that found in the pure manganese perovskites $KMnF_3$ (0.008 \AA) and $RbMnF_3$ (0.006 \AA) by x-ray diffraction as well as to the variation of the divalent cation–fluoride distance in the perovskites: $RbCdF_3$ (0.007 \AA), $RbCaF_3$ (0.008 \AA), $KZnF_3$ (0.006 \AA) and $CsCaF_3$ (0.008 \AA) [16]. It must be emphasized that, though we are implicitly assuming the same ΔR value for the MnF_6^{4-} and the host lattice, this procedure would lead to uncertainties in $\Delta R(300)$ of only about 0.003 \AA if we consider that the local thermal expansion around the Mn is twice or half the host lattice value. However, the 0.007 \AA value is expected to be near the actual value if we take into account that the excitation energy shift for doped perovskites and the pure $RbMnF_3$ and $KMnF_3$ [9] is nearly the same (tables 1 and 2). This estimate will be important to calculate the implicit contribution to the band shift.

3. Analysis and discussion

3.1. Microscopic model

Within a quasiharmonic approximation, the first moment of the excitation and emission bands involving the ${}^4T_{1g}$ state of Mn^{2+} is given by [19]

$$M_1(T) = E_{ZPL}(T) \pm \sum S_i \hbar\omega_i(T) \pm \hbar\omega_{\text{ueff}} \tanh(\hbar\omega_{\text{ueff}}/2kT) \quad (1)$$

where signs + and – are taken for excitation and emission, respectively; $E_{ZPL}(T)$ is the ZPL energy at a given temperature; S_i is the Huang–Rhys factor of the i th linearly coupled phonon of angular frequency $\omega_i(T)$; and the third term represents the thermally averaged energy of the ED origin upon which the phonon sideband is built. The latter term is written in terms of an effective phonon of energy $\hbar\omega_{\text{ueff}}$, according to the thermal dependence of the lifetime $\tau(T)$ measured for the doped crystals [13, 14, 16, 18]. The contribution to the Stokes shift by this ED mechanism, which is $2\hbar\omega_{\text{ueff}}$ at $T = 0 \text{ K}$, becomes zero in the limit $kT \gg \hbar\omega_{\text{ueff}}$ and consequently is responsible for the higher shift experienced by the emission band provided that the ZPLs shift to higher energies upon heating. It is worth noticing that, though the ω_i frequencies are the same for the ground and the excited state within the linear coupling regime, this situation changes a little when the quadratic terms are considered. Through the present study we shall use equation (1) as a reasonable first approximation. The effects of quadratic coupling will however be considered in connection with the temperature dependence of E_{ZPL} . Interestingly, the Mn^{2+} offers the possibility of *separating* the different contributions of equation (1) since the whole emission and excitation bands can be properly obtained from the optical spectra. In fact, if we define the symmetric, $\delta_s(T)$, and antisymmetric, $\delta_a(T)$, parameters by $\delta_s(T) = [M_{1ex}(T) + M_{1em}(T)]/2$ and $\delta_a(T) = [M_{1ex}(T) - M_{1em}(T)]/2$ then we obtain from equation (1)

$$\delta_s(T) = E_{ZPL}(T) \quad \text{and} \quad \delta_a(T) = \sum S_i \hbar\omega_i(T) + \hbar\omega_{\text{ueff}} \tanh(\hbar\omega_{\text{ueff}}/2kT). \quad (2)$$

Within this scheme, δ_s and δ_a represents the ZPL energy and half the Stokes shift, respectively. The accuracy of such an approximation can be checked by comparing the values of $\delta_s(T)$ at low temperatures with E_{ZPL} measured spectroscopically (tables 1 and 2). It can be noticed that the difference $\delta_s(9) - E_{ZPL}$ is always smaller than 50 cm^{-1} . Moreover as the uncertainty involved in the experimental value is about 100 cm^{-1} , the difference $\delta_s(9) - E_{ZPL}$ can be considered as small. Thus the validity of equation (1) for analysing the experimental first moments of the excitation and emission bands is certainly supported by this result. The small deviations between $\delta_s(9)$ and E_{ZPL} found along the series can be associated either with slight deviations of the ground- and excited-state vibrational frequencies or with the lack of instrumental correction. The variations of these parameters from 9 K to T are given by

$$\begin{aligned} \Delta\delta_s(T) &= \delta_s(T) - \delta_s(9) = \Delta E_{ZPL}(T) \\ \Delta\delta_a(T) &= \delta_a(T) - \delta_a(9) = \sum \Delta\{S_i\hbar\omega_i(T)\} - 2\hbar\omega_{\text{eff}}/[\exp(\hbar\omega_{\text{eff}}/kT) + 1]. \end{aligned} \quad (3)$$

The use of these parameters is important in order to minimize the effects due to variations of the excited- and ground-state phonon energies. In the second equation, we neglect the variation of $\hbar\omega_{\text{eff}}$ with temperature given that the energy shift for phonons having energies smaller than 300 cm^{-1} is less than 5 cm^{-1} in the 100–300 K range as measured by IR spectroscopy in the RbCaF_3 , RbCdF_3 and KZnF_3 fluoroperovskites [20]. Table 2 collects the values of these parameters at 300 K obtained from the experimental data of table 1. It must be observed that, at variance with the moment values, $M_{1\text{ex}}$ and $M_{1\text{em}}$, strongly dependent on R , the thermal shifts, $\Delta\delta_s(T)$ and $\Delta\delta_a(T)$, are similar for all crystals independent of their R value and have average values of $+300$ and -150 cm^{-1} at 300 K, respectively.

Both the sign and the magnitude of $\Delta\delta_a(300)$ are well explained through equation (3). In fact, the more relevant contribution to $\Delta\delta_a(300)$ comes from the ED phonon assistance mechanism, which gives a shift of -115 cm^{-1} practically for any value of $\hbar\omega_{\text{eff}}$ in the $220\text{--}320 \text{ cm}^{-1}$ range. The remaining -35 cm^{-1} can be accounted for from the first term of equation (3), by considering that the Stokes shift, $\sum S_i\hbar\omega_i(T)$, can be described by one effective phonon as $S\hbar\omega$ using $S \sim 1\text{--}2$ and $\hbar\omega \sim 400\text{--}500 \text{ cm}^{-1}$ as typical values for MnF_6^{4-} [21]. Then we estimate $\Delta\{S\hbar\omega\}$ to be between -25 and -50 cm^{-1} taking into account that the energy shift of the high-frequency Γ_{LO_2} mode measured by IR spectroscopy for KZnF_3 is -25 cm^{-1} from 100 to 300 K [20], and assuming that the effective Huang-Rhys factor does not change significantly in this temperature range. Therefore both contributions reasonably account for the experimental value $\Delta\delta_a(300) = -150 \text{ cm}^{-1}$. This result also confirms the importance of the phonon assistance mechanism for explaining the different thermal shift experienced by the emission and excitation bands associated with ED transitions.

The variation of the ZPL energy with the temperature, i.e. $\Delta\delta_s(T)$, is somewhat more difficult to estimate. In fact, taking the ZPL energy as a thermodynamic variable, its temperature dependence at constant pressure contains two main contributions:

$$(\partial E_{ZPL}/\partial T)_P = (\partial E_{ZPL}/\partial T)_v + (\partial E_{ZPL}/\partial R)_T(\partial R/\partial T)_P \quad (4)$$

which are known as the explicit and implicit terms, respectively. In the present case, the implicit contribution can be easily estimated since we know the variation of E_{ZPL} with R and also $\Delta R(300)$. Taking the experimental values, $\partial E_{ZPL}/\partial R = +18\,700 \text{ cm}^{-1} \text{ \AA}^{-1}$ and $\Delta R(300) = 0.007 \text{ \AA}$, we obtain $\Delta E_{ZPL}(300) = +130 \text{ cm}^{-1}$, which represents 43% of the total contribution $\Delta\delta_s(300)$, in agreement with previous findings on the first ${}^6\text{A}_{1g} \rightarrow {}^4\text{T}_{1g}$ absorption band maximum of RbMnF_3 and KMnF_3 [9]. This result clearly points out that both the explicit and implicit terms of equation (4) are similar and play an important role

in the thermal band shift for these strongly $10Dq$ -dependent transitions. Accordingly, the remaining 170 cm^{-1} must correspond to the explicit term, which should have the same sign as the implicit contribution. This result contrasts with that observed for the Cr^{3+} and V^{2+} R lines where the thermal shift of -17 cm^{-1} in the 4–300 K range was mostly explained by the explicit contribution in terms of small quadratic couplings revealing ground-state phonon energies slightly higher than those for the excited state [22]. In such a situation, the thermal dependence of the ZPL energy at constant volume is given by

$$E_{\text{ZPL}}(T) = E_{\text{ZPL}}(0) + \sum (\hbar\omega_i^{\text{ex}} - \hbar\omega_i^{\text{gr}})n_i \quad (5)$$

where $E_{\text{ZPL}}(0)$ is the ZPL transition energy at 0 K; $\hbar\omega_i^{\text{ex}}$ and $\hbar\omega_i^{\text{gr}}$ are the i th phonon energy in the excited and ground states, respectively; and $n_i = [\exp(\hbar\omega_i^{\text{ex}}/kT) - 1]^{-1}$ is the corresponding Bose–Einstein occupancy factor. It must be observed that equation (5) has been obtained by considering all transitions between vibronic wavefunctions with the same quantum numbers for the excited and the electronic ground states. Writing the quadratic coupling term as $\sum B_{kl}Q_kQ_l$, equation (5) arises from considering the effects of diagonal terms B_{kk} . The non-diagonal terms $B_{kl}(k \neq l)$ have an important influence upon the second moment and thus the bandwidth but not on the first moment [23, 3, 4]. Note that equation (5) predicts a red or blue shift upon increasing temperature depending on whether the excited-state phonon frequency is smaller than the ground-state one or vice versa. The crucial point for estimating the explicit term is just knowing the value $\delta\omega_i = \omega_i^{\text{ex}} - \omega_i^{\text{gr}}$ for each quadratically coupled mode. Although this information is often hidden in the phonon sidebands, we can extract some interesting conclusions analysing the fine peak structure showed by the low-temperature emission and excitation spectra of the $KMgF_3:Mn^{2+}$ crystal [17, 18]. Before this, it must be noted that the positive sign of this shift in our crystals is a direct consequence of the *hardening* of some vibrations in the ${}^4T_{1g}$ excited state of Mn^{2+} .

3.2. The nature of vibrational modes seen in the optical spectra

The evaluation of equation (5) requires knowledge of the changes experienced by the vibrational frequencies when a complex like MnF_6^{4-} goes from the ground to a given excited state. Some partial information about it can be achieved by looking at the vibrational features reflected in excitation and emission spectra. By virtue of this fact it becomes necessary to discuss the *nature* of such features. Sometimes they are associated with internal modes of the complex while in other cases they are assigned to extended modes of the host lattice. To be more specific in the present analysis let us start with the case of an isolated octahedral MX_6 complex. It is well known that, in the optical transition $|\varphi_g\rangle \rightarrow |\varphi_e\rangle$ between the ground and an excited state, sharp progressions associated with a vibrational mode of the complex, Q , can appear, provided $\Gamma_e \times \Gamma_g \supset \Gamma_Q$ is verified. This selection rule means that the symmetric a_{1g} mode can always give rise to progressions. Moreover if the excited state is an orbital triplet, progressions related to the stretching e_g and the bending t_{2g} modes can also appear. Furthermore for forbidden $d \rightarrow d$ transitions in O_h symmetry there are also sharp features associated with *odd* local phonons only partially enabling the transition. Such peaks are the ‘false origins’ upon which the progressions (involving even modes) are built. Though MX_n complexes are observed *embedded* in a given lattice the preceding description involving only internal modes of the complex explains the main experimental features displayed by the low-temperature spectra of some systems. This situation is encountered for instance in the case of Cr^{3+} -doped A_2BMX_6 elpasolites ($A, B =$ monovalent cation; $M =$ trivalent cation) [24–30]. In this lattice the MX_6 octahedra are well separated. At the same time the internal modes of the MX_6 complex become *transverse* lattice modes of the lattice at

$k = 0$. In other cases the complex appears to be significantly decoupled from the rest of the lattice and thus the main vibrational features observed in optical spectra are again local modes of the MX_n complex. An example of this is Cr^{3+} -doped fluoroperovskites [31]. In this case the decoupling from the rest of the lattice is favoured by the higher charge of Cr^{3+} compared to that of the host cation. Another example of high decoupling corresponds to the $\text{CuX}_4(\text{NH}_3)_2^{2-}$ centre embedded in NH_4X ($\text{X} = \text{Cl}, \text{Br}$) [32, 33]. In this case where Cu^{2+} is located interstitially the Raman spectrum reveals the existence of two sharp a_{1g} modes associated with the Cu-NH_3 and Cu-X vibrations, respectively. As the frequency of the latter lies in the domain corresponding to host lattice vibrations, it is the fingerprint of a centre substantially decoupled from the rest of the lattice. In the case of divalent transition metal impurities (like Mn^{2+} , V^{2+} , Ni^{2+} , ...) doped fluoroperovskite, the vibrational structure seen in optical spectra has been associated with lattice modes of the host lattice [16, 18, 34]. For instance the low-temperature emission spectrum of $\text{KMgF}_3:\text{Mn}^{2+}$ displays a vibrational progression involving a frequency $\hbar\omega_g = 570 \text{ cm}^{-1}$ [18]. This value can hardly be related to a local a_{1g} or e_g mode of the MnF_6^{4-} complex. In fact $\hbar\omega(a_{1g}) = 220 \text{ cm}^{-1}$ for systems involving isolated MnCl_6^{4-} units [35]. Thus taking into account that the replacement of Cl by F as ligand increases the force constant by a factor of 1.7, a figure close to $\hbar\omega(a_{1g}) = 400 \text{ cm}^{-1}$ for the isolated MnF_6^{4-} complex can be expected. Such a value coincides with the estimate of Solomon and McClure [21, 36] from the electronic spectra of RbMnF_3 and lies between the two highest energy peaks of the infrared spectrum of KMgF_3 at 478 and 300 cm^{-1} [37]. The corresponding TO_3 and TO_2 transverse modes at $k = 0$ (Γ point of the Brillouin zone) involve the stretching of the Mg-F bonds [37, 38].

The significant discrepancy between the $\hbar\omega(a_{1g}) = 400 \text{ cm}^{-1}$ expected for the a_{1g} mode of the isolated MnF_6^{4-} complex and the experimental value $\hbar\omega_g = 570 \text{ cm}^{-1}$ can however be understood by accepting that the mode seen in the emission spectrum of $\text{KMgF}_3:\text{Mn}^{2+}$ has a relation with the *longitudinal* LO_3 branch of the KMgF_3 lattice [18] where the highest frequencies in the dispersion curve are involved [37]. In particular, the highest frequency of the LO_3 branch appears at the Γ point of the Brillouin zone, its value being equal to $\hbar\omega(\text{LO}_3, \Gamma) = 590 \text{ cm}^{-1}$ from the calculations reported by Salaun *et al* [38]. Along the ΓX direction the frequency variation is relatively smooth; the value corresponding to the X point is equal to $\hbar\omega(\text{LO}_3, \text{X}) = 547 \text{ cm}^{-1}$. As regards the local behaviour around the divalent ion, the $k = 0$ mode of the LO_3 branch in KMgF_3 behaves as a combination of the a_{1g} and e_g modes of the MgF_6^{4-} complex. As is well known a vibrational mode belonging to a longitudinal branch (like the LO_3 branch of KMgF_3) is in general hardened with respect to the corresponding transverse branch because of the electric field created by the displacement of the whole ions [39]. In the case of KMgF_3 the LO_3 - TO_3 energy difference is particularly high in the ΓX direction [38]. Although the present arguments support a relevant connection between the impurity mode associated with $\hbar\omega_g = 570 \text{ cm}^{-1}$ (in the emission spectrum of $\text{KMgF}_3:\text{Mn}^{2+}$ [18]) and the LO_3 branch of KMgF_3 , we cannot conclude that such a mode (though extended and with a very similar frequency) is just a pure mode of the lattice. This conforms to the highly localized character of electronic states associated with the impurity, implying that relative changes in the frequency of a given lattice mode would be of the order of N_m^{-1} (N_m being the number of lattice cells). The excitation spectrum of $\text{KMgF}_3:\text{Mn}^{2+}$ [17] reveals however that the progression of 570 cm^{-1} in the emission [18] is now of 540 cm^{-1} . This *noticeable shift* between both frequencies indicates that the vibrational frequency observed in optical spectra indeed feels the electronic state of the impurity. This situation is of course observed in cases where the electron-phonon coupling

is made with the modes of the complex, but as explained before it is not expected when coupling occurs with an extended mode of the pure lattice. Therefore the only way to understand the experimental results on $KMgF_3:Mn^{2+}$ is by assuming that the referred mode seen through emission and excitation spectra is extended but its amplitude on the complex is much bigger than that for a normal mode of the host lattice. Designating in a simple way by U_c and $U_{r,i}$ the amplitudes on the complex and on the atom i belonging to the rest of the lattice, then $|U_{r,i}| \approx 1/N_m$ while $|U_c|^2$ can be comparable to $\sum_i |U_{r,i}|^2$. In other words the vibrational mode involved in excitation and emission spectra of $KMgF_3:Mn^{2+}$ would be a kind of resonant mode [40] which though *extended* can have a frequency *sensitive* to the electronic state of the MnF_6^{4-} complex. A tentative model of this impurity mode is depicted in figure 1.

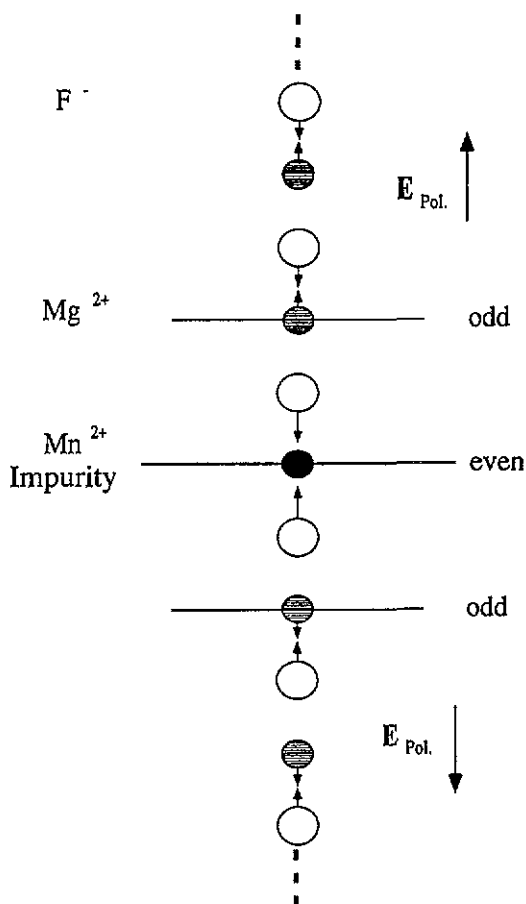


Figure 1. Tentative model of the impurity mode corresponding to $\hbar\omega_g = 570 \text{ cm}^{-1}$ in the emission spectrum of $KMgF_3:Mn^{2+}$. Mn is at rest and the two F^- axial ligands display an even stretching motion around the impurity. The atomic displacements in the upper and lower parts are similar to those corresponding to the $LO_3(\Gamma)$ phonon of $KMgF_3$. Note that the amplitude progressively decreases as far as the lattice ions are more separated from Mn^{2+} . The dipole moment per unit cell is positive (negative) in the upper (lower) part of the drawing.

The softening of the highest energy mode is also observed in $RbCdF_3:Mn^{2+}$, $RbCaF_3:Mn^{2+}$ and $CsCaF_3:Mn^{2+}$ when comparing the emission and excitation bandwidths

as well as their corresponding variation from 9 to 300 K (table 1). The $T = 9$ K bandwidth is typically about 1000 cm^{-1} for excitation and 1300 cm^{-1} in emission, their values increasing 300 and 430 cm^{-1} from 9 K to 300 K, respectively. Therefore, these data reflect that the effective phonon energies associated with ligand field distortions of a_{1g} and e_g symmetry in the electronic ground state are clearly higher than those in the excited state (table 2), according to the spectroscopic observations. These effective frequencies are estimated through the *temperature dependence* of the excitation and emission bandwidths, respectively, by the equation:

$$H(T) = H(0)[\coth(\hbar\omega_{\text{eff}}/2kT)]^{1/2}.$$

The resonant character is also present in other vibrational features seen in the optical spectrum of $\text{KMgF}_3:\text{Mn}^{2+}$ [17, 18]. As reported in [18] there are peaks in the emission spectrum appearing at 137, 223 and 367 cm^{-1} from the ZPL. Such peaks have been associated with the $\text{LA}(X)$, $\Gamma_{25}(t_{2u})$ and $\text{LO}_2(t_{1u})$ lattice modes of KMgF_3 and appear at 149, 256 and 401 cm^{-1} , respectively, in the ${}^6A_{1g} \rightarrow {}^4T_{1g}$ excitation band. At this stage, it is worth mentioning that the assignment of the vibrational fine structure and the corresponding vibrational frequencies derived from the luminescence spectrum at 5 K [18] agree with the phonon dispersion curves recently obtained by Salaun *et al* for KMgF_3 using inelastic neutron scattering and IR data [38].

The resonant character involved in the vibrational modes of $\text{KMgF}_3:\text{Mn}^{2+}$ seen through optical spectra help us to understand the *sign* of the shift observed in the frequency when we go from the ground to the ${}^4T_{1g}$ excited state of MnF_6^{4-} . Let us discuss this point in some detail. For transition metal complexes a transition $t^m e^n \rightarrow t^{m-p} e^{n+p}$ gives rise to a metal–ligand distance, R , longer in the excited state than in the ground state *provided* that p is *positive*. A transition of this kind is for instance the first excitation ${}^4A_2(t^3) \rightarrow {}^4T_2(t^2e)$ observed for CrX_6^{3-} ($X = \text{halide}$) complexes, thus involving the transformation of an antibonding π -electron into an antibonding σ -electron. Such a transformation favours an increase of R and, at the same time, a softening of the *complex frequencies* so that a given frequency, ω_g , in the ground state is higher than ω_e corresponding to the excited state. Therefore if the electron–phonon coupling occurs essentially with local modes of the complex, the frequency, ω_g , seen in emission spectra is higher than the corresponding one, ω_e , detected in the excitation spectra. A good example of this behaviour has been found in cases like $\text{NH}_4\text{Cl}:\text{Cu}^{2+}$ [32, 33], $(\text{N-mph})\text{CuCl}_4$ [41] or K_2PtCl_4 [42].

In the case of an *isolated* MnF_6^{4-} complex the first transition is ${}^6A_{1g}(t^3e^2) \rightarrow {}^4T_{1g}(t^4e)$ and thus in principle R would be smaller for the excited state. This behaviour is actually obtained in the calculation by Luaña *et al* [43]. These authors find that the difference between R_g and R_e (corresponding to the metal–ligand distance for the ground and excited state respectively) is about 0.07 \AA . Moreover in such a calculation they find that $\omega({}^6A_{1g})$ experiences a relative increase of 3% on going from the ground to the ${}^4T_{1g}$ state. This idea is confirmed experimentally in the case of Na_6MnCl_8 where the MnCl_6^{4-} octahedra are well separated and the vibrational modes of the complex also become lattice modes at $k = 0$. In this case $\hbar\omega_g = 214\text{ cm}^{-1}$ while it becomes about 3% higher in the ${}^4T_{1g}$ first excited state [35].

Therefore it now becomes clear that the negative value $\hbar(\omega_e - \omega_g) = -30\text{ cm}^{-1}$ observed for the highest energy mode in $\text{KMgF}_3:\text{Mn}^{2+}$ cannot be understood on the preceding grounds. By contrast it can be a signature of a resonant mode such as is the value of ω_g . It can be thought that the frequency of a resonant mode would depend on the coupling between the vibrations in the complex with those involving ions of the rest of the lattice. Such a coupling would of course be dependent on the electronic state of the complex. Though

this picture provides a reasonable qualitative explanation about the vibrational features seen in Mn^{2+} -doped fluoroperovskites, additional information is required to settle definitely the present problem.

It is important to realize that odd-parity vibrations of the MnF_6^{4-} complex such as the t_{2u} and t_{1u} modes can be coupled quadratically in spite of the fact that their linear coupling is not symmetry-allowed. In particular, this effect can deeply influence the thermal band shift for temperatures below 300 K if low-energy modes are involved. Elpasolites doped with Cr^{3+} are clear examples of this behaviour. A different frequency for the ground and excited electronic state of Cr^{3+} has been observed spectroscopically for odd-parity vibrations of low energy in the Cr^{3+} -doped $Cs_2NaInCl_6$ [26] and K_2NaGaF_6 [25] crystals. The vibrational fine structure in the origin of the ${}^4A_{2g} \rightarrow {}^4T_{2g}$ absorption and luminescence bands indicates that the octahedral t_{2u} local mode of $CrCl_6^{3-}$ is the most efficient enabling ED intensity to the transition. The enhanced ED false origins upon which the phonon sideband is made are displaced from the pure magnetic dipole origins 100 cm^{-1} and 120 cm^{-1} in absorption and luminescence, respectively (see figures 2 and 3 of [26]). Similar results have also been found in $K_2NaGaF_6:Cr^{3+}$ from magneto-optical studies [25] where the ground-state t_{2u} energy, $\hbar\omega_g = 200\text{ cm}^{-1}$, is greater than the excited-state one, $\hbar\omega_e = 160\text{ cm}^{-1}$. Thus the relevance of these modes to the thermal shift should not be ruled out *a priori*.

The analysis of the optical spectra of $KMgF_3:Mn^{2+}$ [17, 18] provides useful information about these quadratic couplings. The observed odd-parity $\Gamma_{25}(t_{2u})$ and $LO_2(t_{1u})$ energies, $\hbar\omega_e = 256$ and 401 cm^{-1} ($\hbar\omega_g = 223$ and 367 cm^{-1}), respectively, clearly indicate that these modes have excited-state frequencies which are neatly higher than the ground-state ones by contrast to the replicas of 570 cm^{-1} in emission and 540 cm^{-1} in excitation found for the high-energy even-character mode. It must be noted that the different behaviour exhibited by the low-energy modes of the Cr^{3+} and Mn^{2+} complexes in the ground and the first excited states is responsible for the opposite sign of both the explicit and implicit contributions to the thermal shifts. The temperature dependence of the ${}^4A_2 \rightarrow {}^4T_2$ transition in $Al_2O_3:Cr^{3+}$ [44] and the present data confirms this behaviour.

3.3. Quantitative estimates of the thermal shift

The correlation between a local and a phonon description can be made on the basis that quadratic coupling through phonons is possible whenever the ligand field distortion around the Mn^{2+} induced by the phonon transforms as one of the quadratically coupled vibrational local modes of O_h symmetry. If we denote by $\delta\omega_i = \omega_{ie} - \omega_{ig}$ the difference between the excited- and ground-state quadratic couplings for the i th phonon mode of a given optical branch, then the contribution to the ZPL thermal shift will be

$$\Delta E_{ZPL} = \sum_i n_i \hbar \delta\omega_i = c \sum_i n_i \hbar \omega_i$$

provided that $\delta\omega_i/\omega_i = c$ along the N_m phonons of the branch. For degenerate phonons or slight phonon dispersion, this contribution equals $cN_m(n_i\hbar\omega_i)$ and therefore would be similar to that corresponding to one strongly coupled resonant phonon of the same frequency whenever the ground state to excited state frequency difference, $\delta\omega = \omega_e - \omega_g$, was similar to $cN_m\omega$. It means that the contribution to the ZPL thermal shift from N_m weakly coupled phonons is similar to that of one resonant mode provided that its quadratic coupling spreads out over the N_m phonons of the optical or acoustic branch.

Consequently, the thermal dependence of the ZPL energy has a very simple analytical equation either for resonant modes or in a pure phonon description assuming *weak* dispersion

within the optical branches and the commonly used approximation, $\delta\omega_i/\omega_i = c_i$; now i represents the i th phonon branch. So

$$\Delta E_{ZPL} = 3c \int_0^{\omega_D} \hbar\omega\rho(\omega)n(\omega) d\omega + 3kT \sum_i c_i \frac{x_i}{\exp(x_i) - 1} \quad (6)$$

where $c = \delta\omega/\omega$ for the acoustic phonons; $\rho(\omega)$ is the phonon state density; $n(\omega)$ is the Bose-Einstein factor; ω and ω_D are the phonon and Debye angular frequencies, respectively; the factor 3 accounts for the longitudinal and the two transverse modes; and $x_i = \hbar\omega_i/kT$. The two terms of equation (6) represent the contribution from the acoustic phonons and the resonant modes (or optical branches), respectively. Note that the acoustic phonons play an important role in the thermal shift due to their low frequencies. The first term of equation (6) is basically the same as employed elsewhere [2-4] for explaining the thermal shifts of the $\text{Cr}^{3+}R$ lines.

For MnF_6^{4-} complexes in fluoroperovskites, ΔE_{ZPL} can be evaluated through equation (6) taking into account that there are 15 vibrational modes in the perovskite structure; three of them spread over the acoustic branches, while the remainder are resonant modes in different optical branches. Although a precise calculation of $\Delta E_{ZPL}(300)$ requires knowledge of ω_i and $c_i = \delta\omega_i/\omega_i$ for each mode, its final value must not change significantly for small deviations of the actual ω_i and c_i values.

Therefore, we can estimate the explicit contribution to $\Delta E_{ZPL}(300)$ from the vibrational frequencies observed in $\text{KMgF}_3:\text{Mn}^{2+}$ taking values of $\hbar\omega$ and $\delta\hbar\omega$ for the three $t_{1u} + t_{2u}$ resonant modes of $\hbar\omega = 570 \text{ cm}^{-1}$ ($\delta\hbar\omega = -30 \text{ cm}^{-1}$) for t_{1u}^3 , 367 cm^{-1} ($+34 \text{ cm}^{-1}$) for t_{1u}^2 , 137 cm^{-1} ($+12 \text{ cm}^{-1}$) for t_{1u}^1 and 223 cm^{-1} ($+33 \text{ cm}^{-1}$) for t_{2u} . From the second term of equation (6), we finally obtain $\Delta E_{ZPL}(300) = +105 \text{ cm}^{-1}$ due to the resonant modes. It must be pointed out that the contribution from the *lowest* energy modes, $t_{1u}^1 + t_{2u}$, is *almost* 90% of this shift, thus indicating that despite the high-energy modes being the most important for the band shape, their contribution to $\Delta E_{ZPL}(T)$ is irrelevant for $T \leq 300 \text{ K}$. This 105 cm^{-1} value corresponds to 60% of the total experimental explicit shift. Analogously, we calculate the contribution from the acoustic phonons (first term of equation (6)) using the Debye approximation:

$$\Delta E_{ZPL}(T) = 3c \int_0^{\omega_D} \hbar\omega\rho(\omega)n(\omega) d\omega = 9cN_m\hbar\omega_D \left(\frac{T}{T_D}\right)^4 \int_0^{T_D/T} \frac{x^3}{e^x - 1} dx \quad (7)$$

where $T_D = (\hbar\omega_D/k)$ is the Debye temperature and $x = \hbar\omega/kT$. We estimate $\omega_D = 4.6 \times 10^{13} \text{ s}^{-1}$ ($T_D = 350 \text{ K}$) for KMgF_3 through the formula $\omega_D = (6\pi^2)^{1/3}v/a$ using values $v = 4.7 \times 10^5 \text{ cm s}^{-1}$ and $a = 3.986 \text{ \AA}$. The sound velocity, v , employed here actually corresponds to the quadratic average of the longitudinal and transverse sound velocities, $v = [(v_l^2 + 2v_t^2)/3]^{1/2}$, obtained through either the elastic constants, $v = [(C_{11} + 2C_{44})/3d]^{1/2}$ ($C_{11} = 1320 \text{ kbar}$, $C_{44} = 485 \text{ kbar}$ and the density $d = 3.2 \text{ g cm}^{-3}$) [38] or their corresponding sound velocities, $v_l = 5.8 \times 10^5 \text{ cm s}^{-1}$ and $v_t = 3.9 \times 10^5 \text{ cm s}^{-1}$ obtained from the phonon dispersion curves [38]. If we take $N_m\delta\omega/\omega = 0.15$, according to the $\delta\omega/\omega$ values measured for the low-frequency modes through the optical spectra, the thermal shift at 300 K from the acoustic modes is $\Delta E_{ZPL}(300) = +60 \text{ cm}^{-1}$. Similar values are obtained using the elastic constants and the lattice parameters of other $\text{ABF}_3:\text{Mn}^{2+}$ crystals. This value, together with the 105 cm^{-1} explicit shift from the resonant modes and the 120 cm^{-1} implicit shift, accounts for a total shift of $+285 \text{ cm}^{-1}$, which is in good agreement with the experimental value, $\Delta E_{ZPL}(300) = 300 \text{ cm}^{-1}$.

4. Conclusions

The present results clearly point out that the thermal shifts experienced by the first excitation and luminescence bands in MnF_6^{4-} complexes are strongly influenced by the ED transition mechanism and both the implicit and the explicit contributions of the ZPL shift. The ED mechanism is mainly responsible for the *different* thermal shift undergone by the excitation and luminescence bands. It has the same sign as the ZPL for emission while the opposite occurs for the excitation band, thus explaining the higher thermal shift found for emission (450 cm^{-1}) than for excitation (150 cm^{-1}).

The implicit contribution is about 40% of the total ZPL shift whereas the remaining 60% is mostly explained in terms of quadratic couplings by the low-energy modes. In particular, it is worth noticing the relevance of the odd-parity modes to the explicit shift despite the fact that they are not linearly coupled to the electronic state. Spectroscopic findings on Cr^{3+} complexes also suggest that the deviations of the ground- and excited-state frequencies of the octahedral t_{2g} modes ($\delta\omega/\omega \sim 0.2$) could be mainly responsible for the opposite sign of the thermal shift exhibited by the ${}^4A_{2g} \rightarrow {}^4T_{2g}$ in these complexes. A precise experimental determination of both the implicit and explicit contributions in CrF_6^{3-} is currently under way. Finally through the present work the different nature of impurity vibrational modes has been discussed. At variance with findings in systems like Cr^{3+} in elpasolite and perovskite lattices where the impurity modes are essentially local modes, it is pointed out that in Mn^{2+} -doped perovskites a distinct situation comes out. As an important conclusion, the analysis carried out here indicates that in $ABF_3:Mn^{2+}$ the impurity modes observed through the emission and excitation spectra are not exactly modes of the pure lattice but display a kind of resonant character. Further work to improve our knowledge about these impurity modes is necessary.

Acknowledgments

Information about the vibrational modes of $KMgF_3$ kindly supplied by Professor M Rousseau is acknowledged. This work has been supported by the CICYT (Project No PB92-0505).

References

- [1] Engleman R 1960 *Mol. Phys.* **3** 23
- [2] McCumber M D and Sturge D E 1963 *J. Appl. Phys.* **34** 1682
- [3] Imbusch G F, Yen W M, Schawlow A L, McCumber D E and Sturge M D 1964 *Phys. Rev. A* **133** 1029
- [4] Di Bartolo B 1968 *Optical Interactions in Solids* (New York: Wiley)
- [5] Henderson B and Imbusch G F 1989 *Optical Spectroscopy of Inorganic Solids* (New York: Oxford University Press)
- [6] Dong-ping M, Xiao-yi H, Ju-rong C, Ji-ping Z and Zheng-gang Z 1993 *Phys. Rev. B* **48** 4302
- [7] Dong-ping M, Xiao-yi H, Ju-rong C, Yan-young L and Ji-ping Z 1993 *Phys. Rev. B* **48** 14067
- [8] Di Bartolo B and Peccei R 1965 *Phys. Rev. A* **137** 1770
- [9] Rodríguez F, Moreno M, Dance J M and Tressaud A 1989 *Solid State Commun.* **69** 67
- [10] Ronda C R, Siekman H H and Haas C 1987 *Physica B* **144** 331
- [11] Darwish S, Abumansoor S and Seehra M S 1986 *Phys. Rev. B* **34** 3198
- [12] Darwish S and Seehra M S 1988 *Phys. Rev. B* **37** 3422
- [13] Marco de Lucas M C, Rodríguez F, Moreno M and Tressaud A 1994 *J. Phys.: Condens. Matter* **6** 6353
- [14] Marco de Lucas M C, Rodríguez F and Moreno M 1993 *J. Phys.: Condens. Matter* **5** 1437
- [15] Studzinski P and Spaeth J M 1986 *J. Phys. C: Solid State Phys.* **19** 6441
- [16] Marco de Lucas M C, Rodríguez F and Moreno M 1994 *Phys. Rev. B* **50** 2760 and references therein
- [17] Ferguson J, Güdel H U, Krausz E R and Guggenheim H J 1974 *Mol. Phys.* **28** 879
- [18] Rodríguez F, Riesen H and Güdel H U 1991 *J. Lumin.* **50** 101

- [19] Jessop P E and Szabo A 1980 *Opt. Commun.* **33** 301
- [20] Ridou C, Rousseau M and Gervais F 1986 *J. Phys. C: Solid State Phys.* **19** 5757
- [21] Solomon E I and McClure D S 1974 *Phys. Rev. B* **9** 4690
- [22] Nelson D F and Sturge M D 1965 *Phys. Rev. A* **137** 1117
- [23] Henry C and Slichter C P 1968 *Physics of Color Centers* (New York: Academic) p 351
- [24] Greenough P and Paulusz A G 1979 *J. Chem. Phys.* **70** 1967
- [25] Dubicki L, Ferguson J and Von Oosterhout B 1980 *J. Phys. C: Solid State Phys.* **13** 2791
- [26] Güdel H U and Snellgrove T R 1978 *Inorg. Chem.* **17** 1617
- [27] Dolan J F, Kappers L and Bartram R H 1986 *Phys. Rev. B* **33** 7339
- [28] Wood A M, Sinkovits, R S, Charpie J C, Huang W L, Bartram R H and Rossi A R 1993 *J. Phys. Chem. Solids* **54** 543
- [29] Marco de Lucas M C, Rodríguez F, Moreno M and Tressaud A 1991 *J. Lumin.* **48 & 49** 553
- [30] Duclos S J, Vohra Y K and Ruoff A L 1990 *Phys. Rev. B* **41** 5372
- [31] Villacampa B, Casas González J, Alcalá R and Alonso P J 1991 *J. Phys.: Condens. Matter* **3** 8281
- [32] Breñosa A G, Moreno M, Rodríguez F and Couzi M 1991 *Phys. Rev. B* **44** 9859
- [33] Couzi M, Moreno M and Breñosa A G 1994 *Solid State Commun.* **91** 481
- [34] Sturge M D 1971 *Solid State Commun.* **9** 899
- [35] Marco de Lucas M C, Rodríguez F and Moreno M 1994 *Phys. Status Solidi b* **184** 247 and references therein
- [36] Chen M Y, McClure D S and Solomon E I 1972 *Phys. Rev. B* **6** 1690
- [37] Nakagawa I, Tsuchida A and Shimanouchi T 1967 *J. Chem. Phys.* **47** 982
- [38] Salaun S, Mortier M, Gesland J Y, Rousseau M and Hennion B 1993 *J. Phys.: Condens. Matter* **5** 7615
- [39] Brüesch P 1982 *Phonons: Theory and Experiments* (Berlin: Springer)
- [40] Barker A and Sievers A J 1975 *Rev. Mod. Phys.* **47** 51
- [41] McDonald R G and Hitchman M A 1986 *Inorg. Chem.* **25** 3273
- [42] Martin D S, Tucker M A and Kassman A J 1966 *Inorg. Chem.* **4** 1682
- [43] Luaña V, Bermejo M, Flórez M, Recio J M and Pueyo L 1989 *J. Chem. Phys.* **90** 6409
- [44] McClure D S 1962 *J. Chem. Phys.* **36** 2757